Provided for non-commercial research and education use.
Not for reproduction, distribution or commercial use.

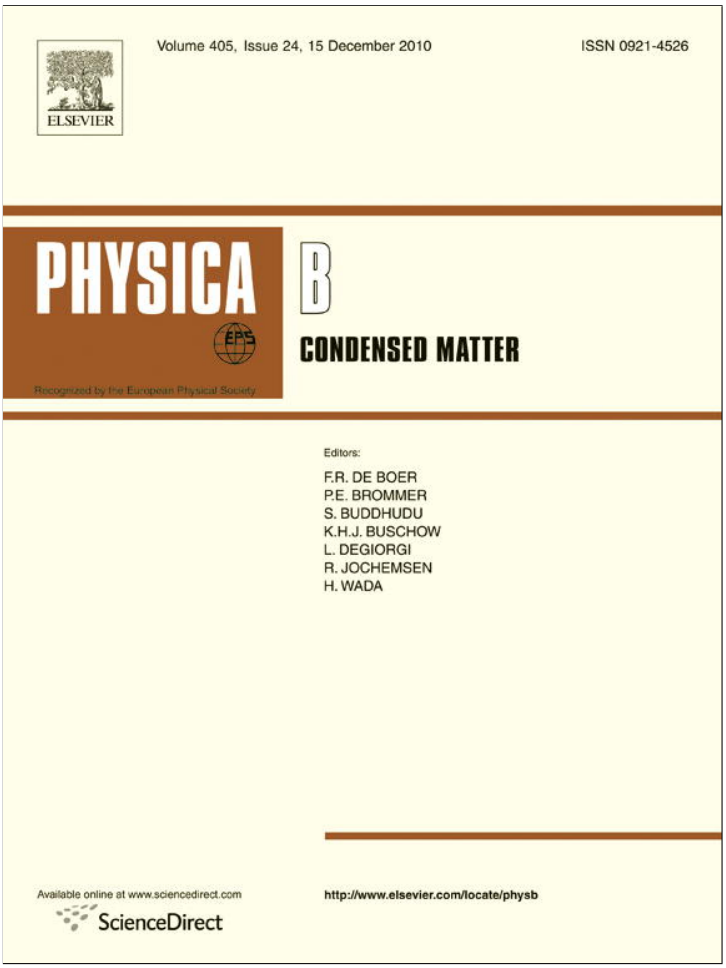

This article appeared in a journal published by Elsevier. The attached copy is furnished to the author for internal non-commercial research and education use, including for instruction at the authors institution and sharing with colleagues.

Other uses, including reproduction and distribution, or selling or licensing copies, or posting to personal, institutional or third party websites are prohibited.

In most cases authors are permitted to post their version of the article (e.g. in Word or Tex form) to their personal website or institutional repository. Authors requiring further information regarding Elsevier's archiving and manuscript policies are encouraged to visit:

http://www.elsevier.com/copyright

Author's personal copy

Physica B 405 (2010) 4970–4977

Contents lists available at ScienceDirect

Physica B

journal homepage: www.elsevier.com/locate/physb

Structural and dynamical properties of the $Cu_{46}Zr_{54}$ alloy in crystalline, amorphous and liquid state: A molecular dynamic study

Camilo Valencia-Balvín [a,b,*], Claudia Loyola [c], Jorge Osorio-Guillén [a], Gonzalo Gutiérrez [c]

[a] Instituto de Física, Universidad de Antioquia, A.A. 1226 Medellín, Colombia
[b] ITM Institución Universitaria, A.A 54959 Medellín, Colombia
[c] Departamento de Física, Facultad de Ciencias, Universidad de Chile, Casilla 653, Santiago, Chile

ARTICLE INFO

Article history:
Received 18 May 2010
Received in revised form
27 September 2010
Accepted 30 September 2010

Keywords:
Molecular dynamics
Metallic glasses

ABSTRACT

Molecular dynamics simulations for the crystal, amorphous and liquid $Cu_{46}Zr_{54}$ alloy were carried out on a system with up to 2000 particles, using a pairwise potential of the Rosato–Guillope–Legrand type. All simulations were done in the microcanonical ensemble, for a initial density of 5.76 g/cm^3, at different temperatures. A detailed analysis has been made by means of the pair-correlation function, coordination number, angle distribution, diffusion coefficient and vibrational density of states. We compared the main peaks of the amorphous phase with experimental data, obtaining a good agreement. The analysis of coordination number for the amorphous phase shows that the main building block of this phase are distorted icosahedron.

© 2010 Elsevier B.V. All rights reserved.

1. Introduction

The strengthening of metallic alloys relative to its pure metal constituents is a subject of great technological and scientific interest, and in particular, bulk amorphous alloys can have excellent strength and corrosion resistance for structural applications. These metallic amorphous phases can be formed if some metallic liquid alloy is cooled at rates which are high enough to suppress crystallization in the melt. Therefore, the liquid-like structural configuration can be frozen into the solid state. The vitrification of a liquid metal was first reported in 1959 by Clement et al. [1] for the Au–Si alloy, when the liquid state of $Au_{75}Si_{25}$ was rapidly quenched. Later, Chen and Turnbull [2] obtained the amorphous ternary alloy Pd–M–Si (with M = Ag, Cu, or Au) in 1969. Just until 1974, a critical casting thickness of 1 mm was obtained for the Pd–T–P (T = Ni, Co, Fe) alloy [3]. In the 1980s, Turnbull et al. [4] produced glassy $Pd_{40}Ni_{40}P_{20}$, by processing it in a boron oxide flux, and the critical casting thickness was increased to 1 cm, the first bulk metallic glass ever obtained. Johnson et al. [5] developed a pentanary alloy based on Zr–Ti–Cu–Ni–Be in 1992, with a critical casting thickness up to 10 cm; the alloy became known as Vitreloy 1, the first commercial bulk metallic glass.

The elastic and mechanical properties of these metallic glasses have been cashing further attention in recent years due to their scientific and engineering significance [6,7]. In general, metallic glasses have a much higher yield point and less ductility, which is thought to be a consequence of the difference in the deformation and fracture mechanisms between metallic glasses and crystalline alloys [8]. However, these amorphous metallic alloys lack tensile ductility, i.e., most metallic glasses loaded with uniaxial tension fail catastrophically [9]. But recently, it has been discovery that some binary metallic glasses support uniaxial tension, e.g. Cu_xZr_{1-x} [8–10].

The formation of possible amorphous phases in binary systems can be seen from its phase diagram, which give us guidelines to find the concentrations necessary to form a metallic glass. For instance, the phase diagram of the Cu–Zr system [11–13] shows that the transition from B2-$Cu_{50}Zr_{50}$ to $Cu_{46}Zr_{54}$ is a eutectic line, a fact that indicates the system goes to one concentration to another through a second order transition which favors the formation of a metallic glass. There have been few experiments to characterize the structure of the $Cu_{1-x}Zr_x$ alloy for different concentrations, such as the measurement of the position of the first-neighbors in the amorphous state [14,15]; the structural evolution of the amorphous state [16] by transmission electron microscopy (TEM), which suggests that the plasticity observed in these alloys is produced by a partial crystallization of the material. Also, by means of neutron inelastic scattering, the dynamical structure factor has been measured at room temperature and the frequency distribution was obtained [17].

Since binary alloys are easier to model than alloys with more elements, this makes Cu–Zr an attractive system to study

* Corresponding author at: ITM Institución Universitaria, A.A 54959 Medellín, Colombia.
E-mail addresses: cavalen@fisica.udea.edu.co, camilovalencia@itm.edu.co (C. Valencia-Balvín).

0921-4526/$ - see front matter © 2010 Elsevier B.V. All rights reserved.
doi:10.1016/j.physb.2010.09.047

Author's personal copy

theoretically. Molecular dynamics (MD) simulations based on the embedded atom method (EAM) have identified local icosahedral order using the Voronoy index [18–20], which provides a good understanding of the mechanical and structural properties of metallic glasses. MD simulations using a more sophisticate potential based on the EAM, where diffraction data from amorphous phases is used [21], have compared the diffusion coefficient, bulk modulus and the pair-correlation function against other types of potential for $Cu_{1-x}Zr_x$. It is found in Ref. [21] that the bulk modulus and the diffusion coefficient are not consistent with the results obtained by EAM simulations, unlike the pair-correlation function which agrees well to these other simulations. Finally, ab initio MD simulations [22,23] have found icosahedral order, like the MD-EAM simulations, a mechanism which could enhance the glass forming ability. Also, the calculated pair-correlation function and the structure factor agree well with the experimental data [23]. However, in spite of the importance of this material, in the literature there are few detailed studies of its structure and dynamics.

Our goal in this paper is to study the structure and dynamics of $Cu_{46}Zr_{54}$ in the crystalline, liquid and amorphous state and to describe its properties at atomic level. In order to do that, we perform MD simulations, using the empirical potential method (EPM). We also use the common neighbor analysis to examine methodically and in detail the structure by the decomposition of the pair-correlation function according to the local environment of the bonded pairs [24] to identify the local order. The paper is organized as follows: in Section 2 we give a short description of the computational details and tools of the structural and dynamical analysis of the calculated alloy. We continue in Section 3 with the analysis of the structural and dynamical properties obtained from the simulation and we end up with some concluding remarks in Section 4.

2. Computational procedure

2.1. Classical molecular dynamics

In the MD method, an important issue is the choice of the interatomic potential. For this simulation, we have adopted the functional form of the many-body force field developed by Rosato and coworkers [25,26] and fitted by Duan et al. [27] for Cu–Zr alloys. This potential has demonstrated to reproduce accurately experimental properties, not only in the solid phase, but also in the liquid as well as in the amorphous state [27,28]. This potential employs the many-body force field form

$$U_{tot} = \Sigma_i U_i = \Sigma_i [E_B^i + E_R^i], \tag{1}$$

$$E_B^i = -\left\{ \Sigma_{i \neq j} c^2 \exp\left[-2q\left(\frac{r_{ij}}{r_0} - 1 \right) \right] \right\}^{1/2}, \tag{2}$$

$$E_R^i = \Sigma_{i \neq j} \frac{1}{2} \varepsilon \exp\left[-p\left(\frac{r_{ij}}{r_0} - 1 \right) \right], \tag{3}$$

where E_B^i and E_R^i (i=Cu,Zr) denote the many-body metallic bonding potential and the pairwise repulsive energy terms, respectively; r_0 is the first-neighbor distance and the other four free-fitting parameters c, q, ε and p are taken from Ref. [27] (see Table 1).

The simulation in this work is done in the microcanonical ensemble (NVE). We have used as starting volume for crystalline $Cu_{46}Zr_{54}$ the value found in Ref. [27] at 300 K and trying to keep the external pressure at 0 GPa, approximately. The MD simulation has been done following these steps: first, in order to get the crystalline, amorphous and liquid phases, we have taken as initial system the $Cu_{50}Zr_{50}$ crystal with the B2 structure, containing 2000 atoms. Then, we have replaced 80 Cu atoms by Zr atoms randomly, obtaining a $Cu_{46}Zr_{54}$ alloy, and finally we have adjusted the alloy volume to the density of 5.79 g/cm^3 in correspondence to the new concentration. Second, we have heated the system from an initial temperature of 300–3000 K doing two temperature controls. Each temperature control has been done scaling the temperature during $5000\Delta t$($\Delta t = 10^{-15}$ s) and relaxing the system during 15 $000\Delta t$. For the first control, we changed the temperature at a rate of 0.34 K/Δt. Then, the last configuration obtained at 2000 K is heated at a rate of 0.2 K/Δt doing the second control and obtaining a system at 3000 K. Third, we cooled the system from 3000 to 300 K taking the same type of temperature control. In this case, we did 11 temperature controls by decreasing the temperature 250 K for each control at a rate of 0.05 K/Δt. Further, for the temperature controls at 1250, 750 and 500 K, the volume is adjusted to keep the pressure at 0 GPa, approximately.

Table 1
Force field parameters used in this simulation Ref. [27].

	r_0 (Å)	ε (eV)	c (eV)	p	q
Zr–Zr	3.2100	0.3688	2.3365	2.0250	7.9273
Cu–Cu	2.6356	0.2149	1.3483	2.7490	10.2215
Cu–Zr	2.9086	0.3615	2.0100	2.7960	8.6020

2.2. Structural analysis

In this section we briefly describe the different structural and dynamical functions that we will use to characterize the difference among alloy states.

2.2.1. The pair-correlation function

The partial pair-correlation function $g_{\alpha,\beta}(r)$ is widely used to describe the atomic structure in crystalline, liquid and amorphous states. This quantity is given by

$$g(r)_{\alpha,\beta} = \frac{\langle n_{\alpha,\beta}(r, r+\Delta r) \rangle}{\rho 4\pi r^2 \Delta r} \frac{V}{N_\beta}, \tag{4}$$

where α, β = Cu, Zr, and $\langle n_{\alpha,\beta}(r, r+\Delta r) \rangle$ denotes the average number of particles of species β surrounding a particle of species α in a spherical shell between r and $r+\Delta r$, and N_β is the total number of particles of species β (being $N = N_\alpha + N_\beta$, the total number of particles in the system). The total pair-correlation function is obtained by

$$g(r) = \sum_\alpha \sum_\beta c_\alpha c_\beta g_{\alpha,\beta}(r), \tag{5}$$

where $c_{\alpha(\beta)} = N_{\alpha(\beta)}/N$ is the concentration of $\alpha(\beta)$ specie.

2.2.2. Nearest-neighbors coordination number

The average coordination number $n_{\alpha\beta}$ is calculated by

$$n_{\alpha\beta} = 4\pi c_\beta n \int_0^R g_{\alpha\beta}(r) r^2 \, dr, \tag{6}$$

where $n = N/V$ is the average number density. This quantity helps us to get more information on short-range correlations.

2.2.3. Angle distribution

A valuable information about the local structural units and their connectivity is provided by the bond-angle distribution $P_{\alpha\beta\gamma}(\theta)$. Bond-angle distribution is obtained from MD trajectories as follows: let us consider the case of a $\beta-\alpha-\beta$ bond angle

Author's personal copy

distribution. In this case, a list of nearest-neighbor atoms of type β around an α atom is constructed. This requires a distance cut-off for the $\alpha-\beta$ separation which is taken to be the position of the first minimum in $g_{\alpha\beta}(r)$. From this nearest-neighbor list, for each α atom, the $\beta-\alpha-\beta$ angle is calculated for all bonds and a histogram is then constructed from an average over all angles involving all α atoms. Next, let us consider an $\alpha-\alpha-\beta$ bond-angle distribution. In this case, two nearest-neighbor distance lists involving atoms α and β around each α atom are constructed. The distances cut-off are the first minimal in $g_{\alpha\alpha}(r)$ and $g_{\alpha\beta}(r)$. Then a histogram is constructed from all $\alpha-\alpha-\beta$ angles. All the other cases are constructed in a similar way.

2.2.4. The common neighbor analysis

The common neighbor analysis (CNA) is a method for analyzing structures by a decomposition of the pair-correlation function (PDF) according to the local environment of the bonded pairs [24]. The first PDF peak, for example, is composed of bonded nearest-neighbor pairs with different environments. Here, the bonded nearest neighbors are those within the radius range from zero to a distance cut-off r_c, where r_c is taken as the position of the first minimum of the total PDF. Each such pair of atoms is systematically classified according to its surroundings in the following way: a set of three indices *jkl* specifies the local environment of the pair; the first index j is the number of neighbors common to both atoms, the second index k is the number of bonds between the common neighbors, the third index l is the number of bonds in the longest continuous chain formed by the k bonds formed between common neighbors. After each pair has been assigned to one of the various *jkl* types, a PDF for each type of pairs can then be obtained and the total PDF is the summation of these pair PDFs.

2.2.5. Diffusion coefficient

The coefficients of self-diffusion were calculated from mean-square displacements. This coefficient gives us a way to quantify the transport of molecules from a region of higher concentration to one of lower concentration by random molecular motion [29]

$$D_\alpha = \lim_{t\to\infty} \frac{\langle r^2 \rangle_\alpha}{6t}, \tag{7}$$

where

$$\langle r^2 \rangle_\alpha = \left\langle \frac{1}{N_\alpha} \sum_{j(\alpha)} [r_j(t+s) - r_j(s)]^2 \right\rangle, \tag{8}$$

$\langle\ \rangle$ means an average over configurations.

2.2.6. Vibrational density of states

The dynamical properties are studied by means of the vibrational density of states $D(\omega)$. We obtain $D(\omega)$, first calculating the velocity autocorrelation functions for species $\alpha(\beta)$,

$$Z_{\alpha(\beta)}(t) = \left\langle \sum_{i=1}^{N} m_{i\alpha} \vec{v}_{i\alpha}(0) \cdot \vec{v_{i\alpha}}(t) \right\rangle, \tag{9}$$

where $m_{i\alpha}$ is the mass of the atom i and specie $\alpha(\beta)$ and $\vec{v}_{i\alpha(\beta)}$ is its velocity. By performing a Fourier transform,

$$D_{\alpha(\beta)}(\omega) = \frac{1}{\sqrt{2\pi}} \int \frac{Z_{\alpha(\beta)}(t)}{Z_{\alpha(\beta)}(0)} e^{-i\omega t}\, dt, \tag{10}$$

the partial $D_{\alpha(\beta)}(\omega)$ is obtained. From this, we obtain the total density of states $D_{\alpha(\beta)}(\omega) = \sum_\alpha c_\alpha D_\alpha(\omega)$ and the total neutron section-weighted one phonon density of states

$$D_{\alpha(\beta)}(\omega) = \sum_\alpha \frac{c_\alpha 4\pi b_\alpha^2}{m_\alpha} D_\alpha(\omega). \tag{11}$$

3. Results

In this section we present the results of our MD simulation for the crystalline, liquid and amorphous states. For each of them,

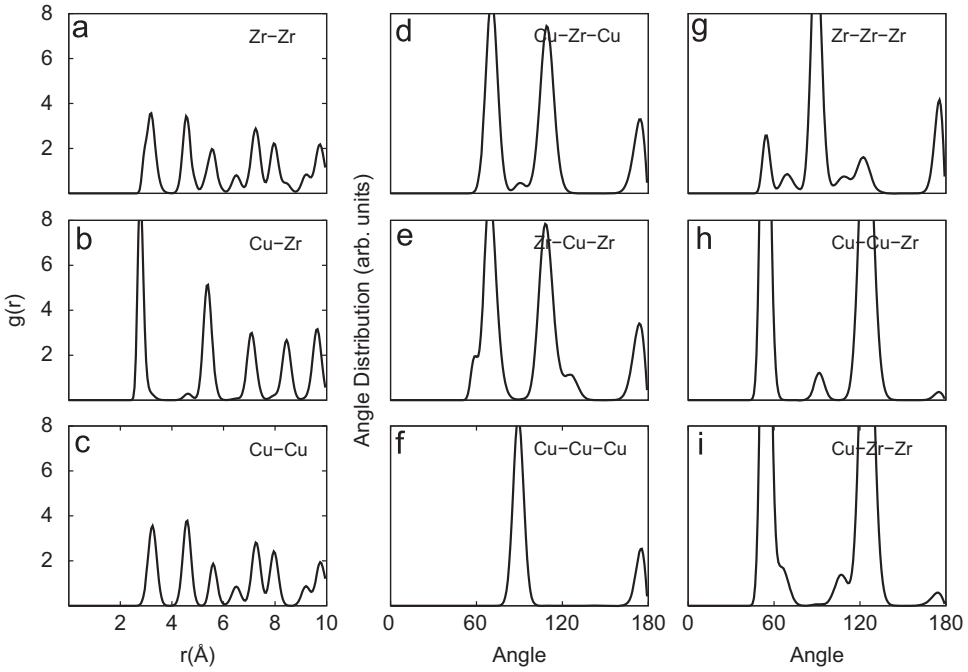

Fig. 1. (a)–(c) Calculated pair-correlation function for $Cu_{46}Zr_{54}$ crystalline phase: the main peaks are located at (a) 3.18 Å for Zr–Zr, (b) 2.76 Å for Cu–Zr and (c) 3.22 Å for Cu–Cu. (d)–(i) Calculated angular distribution for the crystalline phase: the main peaks are located at (d) 70° and 110° for Cu–Zr–Cu and (e) Zr–Cu–Zr, (f) 90° and 175° for Cu–Cu–Cu and (g) Zr–Zr–Zr. Finally, (h) 54° and 125° for Cu–Cu–Zr and (i) Cu–Zr–Zr bond angles.

Author's personal copy

we have studied its structural properties inferred by means of the pair-correlation function, coordination number, angular distribution, common neighbor analysis, diffusion coefficient, and vibrational density states.

3.1. Crystal

We performed the simulation for the disordered structure of $Cu_{46}Zr_{54}$ obtained from B2-$Cu_{50}Zr_{50}$ (see above in Computational Procedure). Figs. 1(a)–(c) present the calculated pair-correlation function for a temperature of around 300 K. It shows the typical peaks of a B2 structure at 3.18 Å for Zr–Zr, 2.76 Å for Cu–Zr and 3.22 Å for Cu–Cu. Also, we can observe from the partial pair-correlation function that the first-nearest neighbor positions are occupied by atoms of different species and the second nearest-neighbor positions are occupied by atoms of the same specie.

The calculated angle distribution is shown in Figs. 1(d)–(i). We have calculated it using the cut-off distance values of 3.7, 3.5 and 3.92 Å for Zr–Zr, Cu–Zr and Cu–Cu, respectively. The angles that form Cu–Zr–Cu and Zr–Cu–Zr bonds have two equal peaks at 70° and 110°. Also, we can see the characteristic peaks of the Cu–Cu–Cu and Zr–Zr–Zr angles have the same maximum of 90° and 175°, which are close to the B2 structure. Finally, the Cu–Cu–Zr and Cu–Zr–Zr bond angles have peaks at 54° and 125°.

In the analysis of the coordination number, we take in all the cases a cut-off radius of 4.0 Å, which is extracted from the first minimum of the pair-correlation function $g(r)$. Figs. 2(a)–(d) show that Cu have five Cu neighbors and eight Zr neighbors.

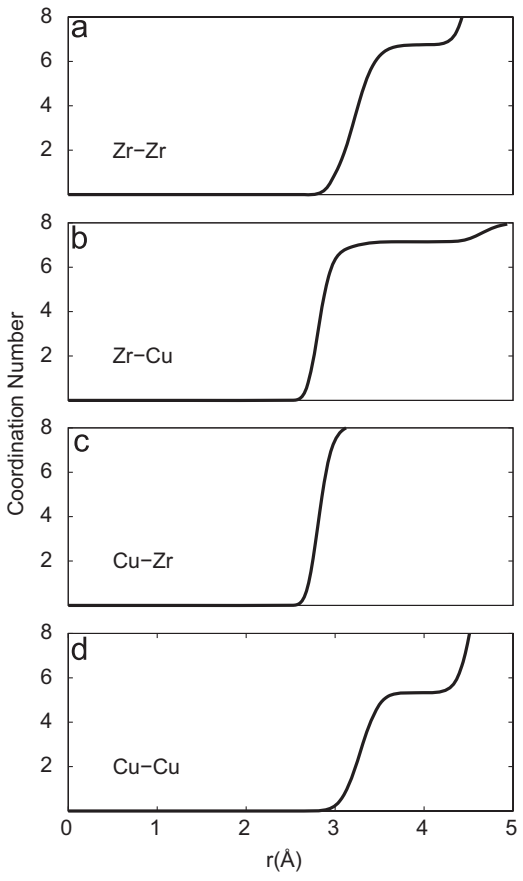

Fig. 2. Calculated coordination number (CN) for $Cu_{46}Zr_{54}$ crystalline phase. (a) Zr–Zr (CN=7), (b) Zr–Cu (CN=7), (c) Cu–Zr (CN=8), and (d) Cu–Cu (CN=5).

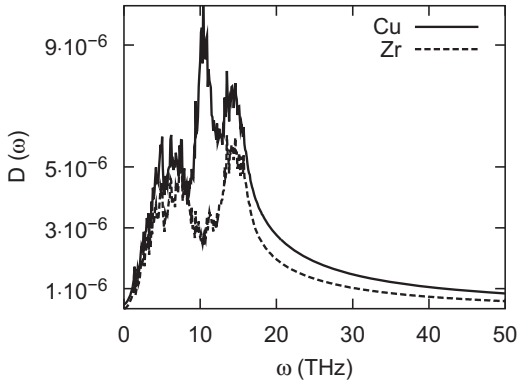

Fig. 3. Calculated vibrational density of states for $Cu_{46}Zr_{54}$ crystalline phase. Solid line represents the partial vibrational density of states for Cu and the dashed line is the partial vibrational density states for Zr.

In the case of Zr, we have seven Zr neighbors and seven Cu neighbors. Finally, Fig. 3 shows the calculated vibrational density of states $D_\alpha(\omega)$ ($\alpha =$ Cu, Zr). We can see the highest peaks for $D(\omega)$ at 12 and 14 THz for Cu and Zr, respectively. These peaks agree well with the ones calculated in Ref. [30] for the $Cu_{50}Zr_{50}$ glass.

3.2. Liquid

Around 2000 K the emergence of broad peaks in the partial-distribution function of the $Cu_{46}Zr_{54}$ alloy (Figs. 4(a)–(c)) shows that the structure has melted and it is in liquid state. For instance, $g(r)_{Cu-Cu}$ indicates a peak at the first-nearest neighbor distance of 2.6 Å, which is close to the value of pure liquid Cu and its amorphous state as well. We can observe that the peaks of the atoms of the same species, i.e. Cu–Cu and Zr–Zr, undergo a shift to the right in comparison to the peaks in $g(r)$ for the crystalline phase. Furthermore, we can note a preference of Cu atoms to be closer between them.

Regarding the angular distribution in the liquid state (Figs. 4(d)–(i)), we have calculated it using cut-off distance values of 4.7, 4.0 and 3.7 Å for Zr–Zr, Cu–Zr and Cu–Cu, respectively. The main peaks are located at 58° and 114° for Cu–Zr–Cu bond angle, 70° and 110° for Zr–Cu–Zr, 58° and 110° for Cu–Cu–Cu and Zr–Zr–Zr, and finally 55° and 110° for Cu–Cu–Zr and Cu–Zr–Zr bond angles. If we compare the liquid phase to the crystalline phase, we can observe that the first and second peaks in the liquid phase for Cu–Zr–Cu and Zr–Cu–Zr bond angles do not match to the crystalline phase, and they are displaced by 12° and 4°, respectively. Also, there is a shift to the right in the first peak of the Cu–Cu–Cu and Zr–Zr–Zr bond angles with respect to the crystalline state by 32°. In the case of the Cu–Cu–Zr bond angle, there is a shift to the right in the first peak of 1° and a shift to the left of 15° for the second peak in comparison to the crystal phase. Finally, for the Cu–Zr–Zr bond angle we can observe that the first peak is located approximately at the same value of the crystalline phase.

The calculated coordination number is shown in Figs. 5(a)–(d). We can observe for all a loss of localization of the neighbors, thus we can certainly conclude that the system is in its liquid phase.

In Fig. 6, we present the calculated diffusion coefficient for Cu and Zr, whose values are 0.061 and 0.051 $Å^2\,fs^{-1}$, respectively. We note that Cu has a greater diffusion coefficient than Zr, i.e., Cu atoms in the liquid have a greater mobility than Zr atoms. This fact could explain why the first-neighbors peak in the pair-correlation function for Cu–Cu in the crystalline phase is displaced

Author's personal copy

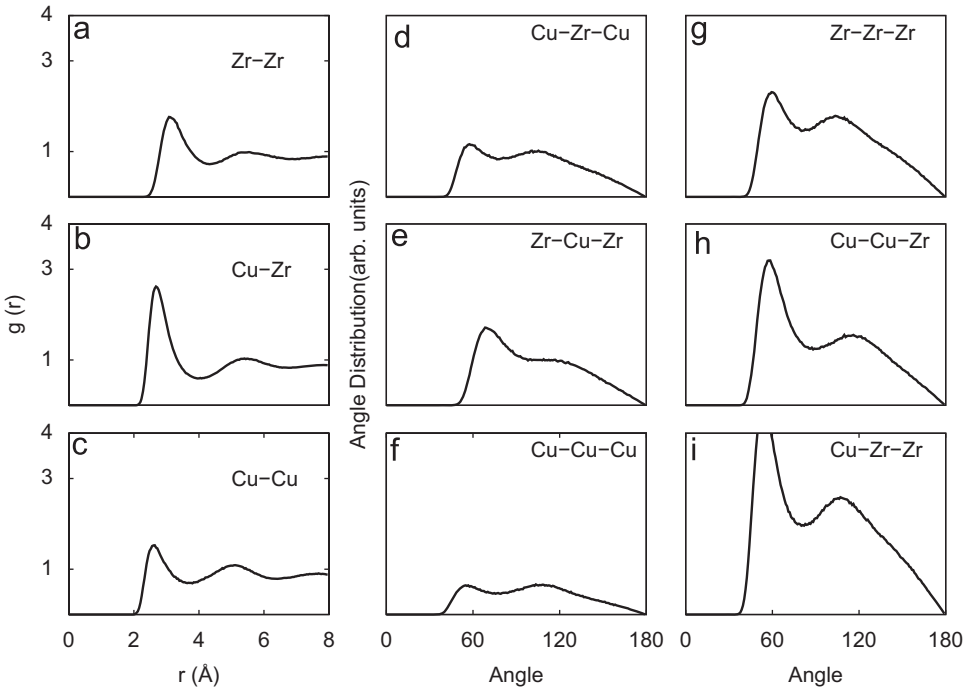

Fig. 4. (a)–(c) Calculated pair-correlation function for $Cu_{46}Zr_{54}$ crystalline phase: two main peaks are located at (a) 3.1 and 5.5 Å for Zr–Zr, (b) 2.7 and 5.2 Å for Cu–Zr, finally (c) 2.6 and 5 Å for Cu–Cu (c). (d)–(i) Calculated angular distribution for the crystalline phase: the main peaks are located at (d) 58° and 114° for Cu–Zr–Cu, (e) 70° and 110° for Zr–Cu–Zr, (f) 58° and 110° for Cu–Cu–Cu and (g) Zr–Zr–Zr. Finally, (h) 58° and 110° for Cu–Cu–Zr and (i) Cu–Zr–Zr bond angles.

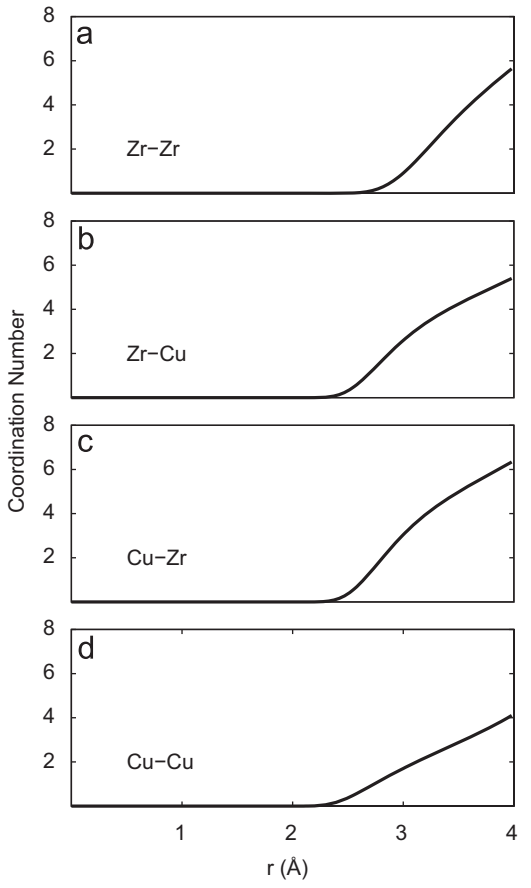

Fig. 5. (a)–(d) Calculated coordination number for $Cu_{46}Zr_{54}$ liquid phase.

towards the left with respect to Cu–Zr and Zr–Zr, when we compare them to its liquid phase and amorphous phase (see next subsection).

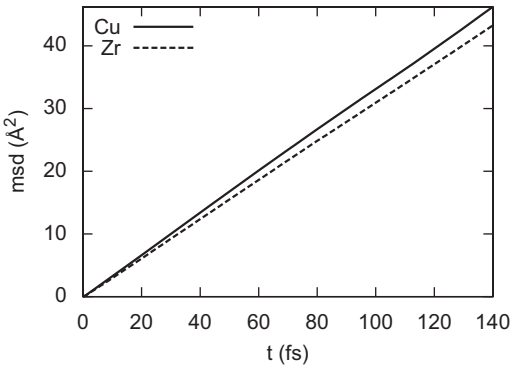

Fig. 6. Calculated diffusion coefficient for $Cu_{46}Zr_{54}$ liquid phase. The diffusion coefficient for Cu (solid line) is 0.061 $Å^2 fs^{-1}$ and for Zr (dashed line) is 0.051 $Å^2 fs^{-1}$.

3.3. Amorphous

Figs. 7(a)–(c) show the calculated pair-correlation function for the amorphous state of $Cu_{46}Zr_{54}$ at a temperature around 300 K. We can see the features of short-range order, where the peaks broad wider than the ones in the crystalline phase. The second, third and further peaks of $g(r)_{Zr-Zr}$, $g(r)_{Cu-Zr}$ and $g(r)_{Cu-Cu}$ are spread almost entirely, showing the formation of an amorphous phase. On the other hand, the first peak of Cu–Zr pairs at 2.7 Å is relatively sharp compared to those of Cu–Cu and Zr–Zr pairs at 2.6 and 3.1 Å, respectively. This suggests a preferred interaction of Cu–Zr atoms in this alloy. The calculated features of the local structure of this metallic glass are compared in Table 2 to experimental values obtained by X-ray diffraction (XRD) and extended X-ray absorption fine structure (EXAFS) techniques [14,15] at room temperature. We can see that the first peak position of the partial pair-correlation presents a small difference: the calculated Cu–Cu pair differs in 2.7% to the XRD measurement for $Cu_{50}Zr_{50}$ and 2.3% to the measured first peak with EXAFS at the

Author's personal copy

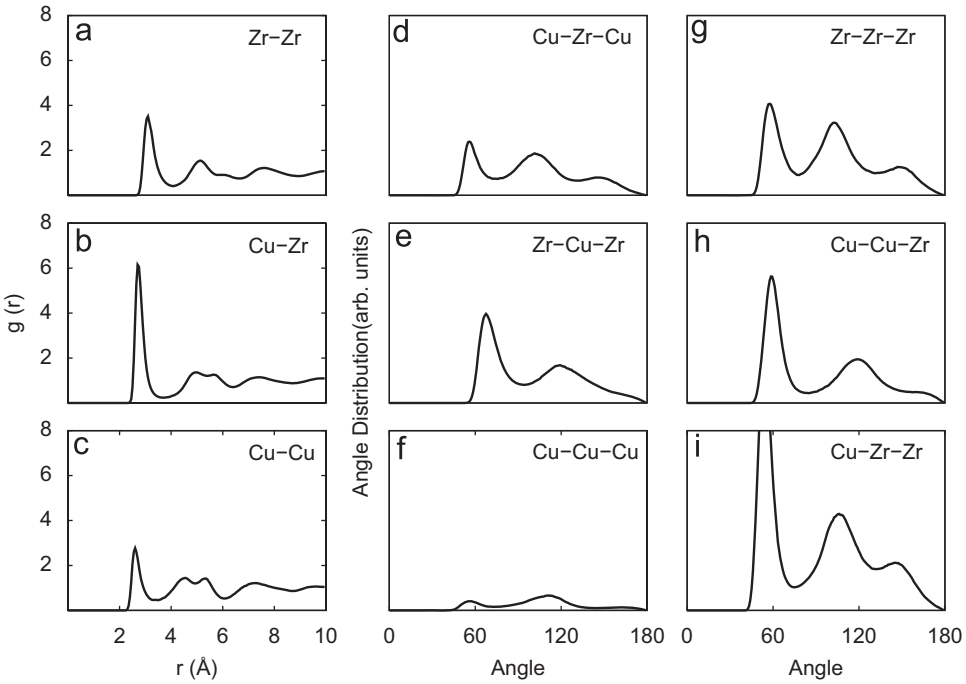

Fig. 7. (a)–(c) Calculated pair-correlation function for $Cu_{46}Zr_{54}$ crystalline phase: two main peaks are located at (a) 3.10 and 5.15 Å for Zr–Zr, (b) 2.70 and 4.95 Å for Cu–Zr and (c) 2.60 and 4.55 Å for Cu–Cu. (d)–(i) Calculated angular distribution for the crystalline phase: the main peaks are located at (d) 56° and 102° for Cu–Zr–Cu, (e) 68° and 120° Zr–Cu–Zr, (f) 56° and 112° for Cu–Cu–Cu, (g) 57° and 103° Zr–Zr–Zr, (h) 60° and 120° for Cu–Cu–Zr and finally (i) 54° and 106° Cu–Zr–Zr bond angles.

Table 2
Experimental and calculated first-peak position for amorphous Cu–Zr alloys.

$Cu_{46}Zr_{54}$	R(Cu–Cu) (Å)	R(Cu–Zr) (Å)	R(Zr–Zr) (Å)
XRD[a]	2.53	2.75	3.15
EXAFS[b]	2.54	2.72	3.14
Amorphous[c]	2.60	2.74	3.1
Amorphous[d]	2.67	2.78	3.22
Amorphous[e]	2.58	2.84	3.17

[a] In this case the composition is $Cu_{50}Zr_{50}$, Ref. [14].
[b] Ref. [15].
[c] This work.
[d] Ref. [27].
[e] In this case the composition is $Cu_{64.5}Zr_{35.5}$, Ref. [21].

same concentration. For the other pairs, we have that Cu–Zr differs in 0.4% and 0.7%, and Zr–Zr differs in 1.6% and 1.3% to the XRD and EXAFS measurements, respectively. We also compared our results with those reported by Mendelev et al. [21,31] for $Cu_{64.5}Zr_{35.5}$ and Duan et al. [27] for $Cu_{46}Zr_{54}$ (Table 1), where it is observed that the first peak positions of the partial pair-correlation distribution are in good agreement to our results.

Next, the calculated angular distribution is shown in Figs. 7(d)–(i). It is observed that the angle distribution becomes more broader with respect to the crystalline phase, furthermore, we can observe that the more pronounced cases are found for Cu–Cu–Cu and Zr–Zr–Zr bond angles. Our results are comparable to those calculated in Ref. [31] for $Cu_{64.5}Zr_{35.5}$ and the *ab-initio* results from Ref. [23] for $Cu_{50}Zr_{50}$, where their calculated angular distribution for Cu–Zr–Cu, Zr–Cu–Zr, Cu–Cu–Cu and Zr–Zr–Zr bond angles show a good agreement with our results.

The calculated coordination number for the amorphous structure is displayed in Figs. 8(a)–(d), where we can observe just one peak in the Zr–Zr, Zr–Cu, Cu–Zr and Cu–Cu pairs; their calculated values are 8.07, 6.57, 7.72 and 3.2, respectively. Our results are consistent with those obtained in Ref. [27], as expected because we have used the same potential, but they differ with

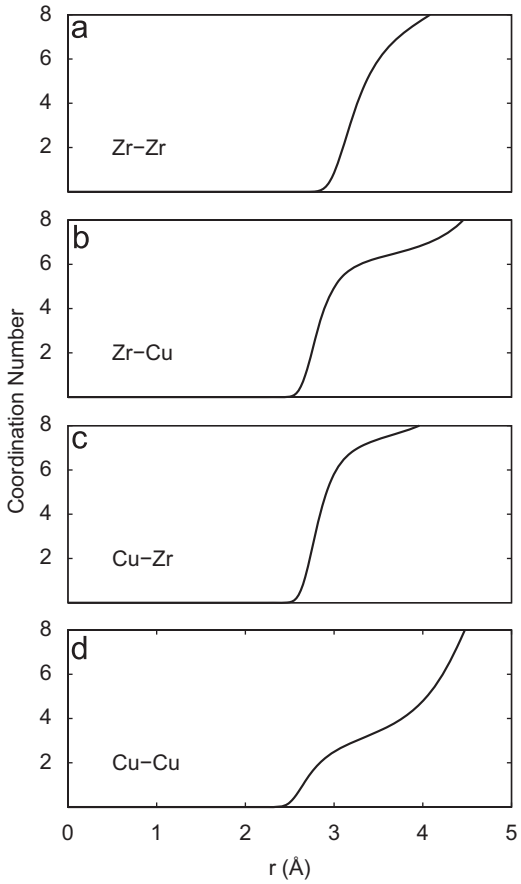

Fig. 8. (a)–(d) Calculated coordination number for $Cu_{46}Zr_{54}$ amorphous phase.

respect to the experimental values (Table 3). To continue with the analysis of the structure of the amorphous state, we can seek the presence of topological short-range order features given by

Author's personal copy

Table 3
First-neighbors for amorphous Cu–Zr alloys: experimental and calculated values at room temperature.

$Cu_{46}Zr_{54}$	N(Cu–Cu)	N(Cu–Zr)	N(Zr–Cu)	N(Zr–Zr)
XRD[a]	5.8	5.6	5.0	5.0
EXAFS[b]	6.0	5.5	5.0	5.0
Amorphous[c]	3.2	7.72	6.57	8.07
Amorphous[d]	3.2	7.6	6.5	9.1

[a] In this case the composition is $Cu_{50}Zr_{50}$, Ref. [14].
[b] Ref. [15].
[c] This work.
[d] Ref. [27].

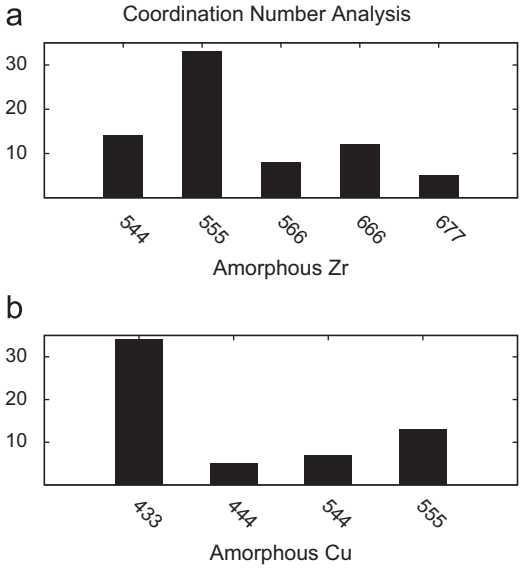

Fig. 9. (a) Calculated histogram for Zr–Zr pair coordination number. The most abundant pairs are 555 and 544, indicating the dominance of perfect icosahedral order and other different type of distorted icosahedral order, respectively. (b) Calculated histogram for Cu–Cu pair coordination number. The most abundant pairs are 433 and 555, indicating the dominance of a type of distorted icosahedral order.

the CNA; which decomposes the first pair-correlation function peak according to the different local environment of the bonded nearest-neighbor pairs (i.e., those within a cut-off distance corresponding to the first minimum of the total pair-correlation function). The calculated CNA is shown in the histogram of Figs. 9(a) and (b), where the relative fractions of the major pairs types (others with small populations are neglected). One can observe that there is partial order in the amorphous structure as follows: in Fig. 9(a) for the Zr–Zr pairs are observe the 555 index, characteristic of a perfect icosahedral ordering and the 544 index [32,33], that represent a different type of distorted icosahedral order. For the Cu–Cu pairs (Fig. 9(a)) are observed the 433 and 555 indexes, which are characteristic of distorted and perfect icosahedral order, respectively. Therefore we can conclude that the local structure of the amorphous state is mostly build up by distorted icosahedron.

Finally, we have also calculated the vibrational density of states $D(\omega)$ for the amorphous phase, as shown in Fig. 10. The more relevant features of $D(\omega)$ are located at 19 and 8 THz for Cu and Zr, respectively. However, when we compare this density states to the crystalline case we can see an almost structureless distribution; which is probably due to the superposition of the frequency spectra of several polycrystalline phases of Cu–Zr, as observed in the experimental data [17]. Also, we have compared

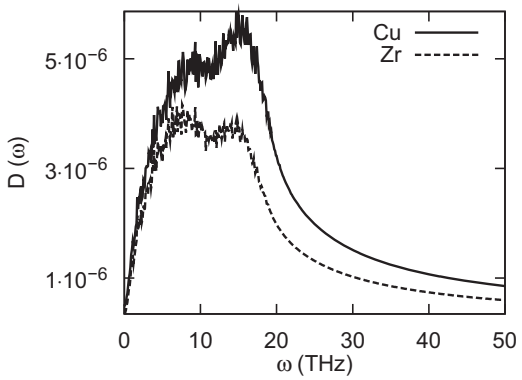

Fig. 10. Calculated vibrational density of states for $Cu_{46}Zr_{54}$ amorphous phase. Solid line represents the partial vibrational density of states for Cu and the dashed line is the partial vibrational density states for Zr.

our calculations with neutron inelastic scattering measurements for the $Cu_{60}Zr_{40}$ glass [34]. The experimental vibrational density of states is consistent with our calculation, showing a lack of structure in the distribution.

4. Conclusion

In summary, we have presented a computer simulation for crystalline, liquid and amorphous $Cu_{46}Zr_{54}$ using the many-body force field potential developed by Rosato–Guillope–Legrand. A detailed study has been made by the analysis of the pair-correlation function, coordination number, angle distribution, common neighbor analysis, diffusion coefficient and vibrational density of states. We have found that our calculated alloy crystal structure and the crystal phase B2 present many structural similarities. We observe a shift of the main peak of the pair-correlation function for the Cu–Cu distance for the liquid state in comparison to the crystalline state, which we attribute to the diffusion coefficient of Cu, which is bigger than in the case of Zr. The local structure of the amorphous state is mostly build up by distorted icosahedron and perfect icosahedron. Also, we have found that in the amorphous phase the main peaks of the calculated pair-correlation function are consistent with the peaks found by XRD and EXAFS experiments.

Acknowledgments

The authors would like to thank the Colombia agency CODI-Universidad de Antioquia (Estrategia de Sostenibilidad Grupo de Materia Condensada-UdeA, 2009–2010) and Project PBCT-Chile Anillo ACT-24 “Computer simulation lab for nanobio materials”.

References

[1] W. Klement, R.H. Willens, P. Duwez, Nature 187 (1960) 869.
[2] H.S. Chen, D. Turnbull, Acta Metall. 17 (1969) 1021.
[3] H.S. Chen, Acta Metall. 22 (1974) 1505.
[4] H. Kui, A.L. Greer, D. Turnbull, Appl. Phys. Lett. 45 (1984) 615.
[5] A. Peker, W.L. Johnson, Appl. Phys. Lett. 63 (1993) 2342.
[6] M. Telford, Mater. Today 1 (2004) 36.
[7] A. Lindsay Greer, Mater. Today 12 (2009) 14.
[8] J. Das, M.B. Tang, K.B. Kim, R. Theissmann, F. Baier, W.H. Wang, J. Eckert, Phys. Rev. Lett. 94 (2005) 205501.
[9] D.H. Xu, Acta Matter. 52 (2004) 2621.
[10] J. Das, S. Pauly, M. Bostrom, K. Durst, M. Goken, J. Eckert, J. Alloys Compd. 483 (2009) 97.
[11] X.C. He, H. Wang, H.S. Liu, Z.P. Jin, Calphad 30 (2006) 367.
[12] H. Okamoto, J. Phase Equilibria Diffus. 29 (2008) 204.

Author's personal copy

[13] X. Ji, Y. Pan, F. Ni, Mater. Des. 30 (2009) 842.
[14] H.S. Chen, Y. Waseda, Status Solidi A 51 (1979) 593.
[15] A. Sadoc, Y. Calvayrac, A. Quivy, M. Harmelin, A.M. Flank, J. Non-Cryst. Solids. 65 (1984) 109.
[16] D.C. Hofmann, G. Duan, W.L. Johnson, Scr. Mater. 54 (2005) 1117.
[17] J.B. Suck, H. Rudin, H.J. Guntherodt, H. Beck, J. Danbert, W. Glaser, Phys. C Solid State Phys. 13 (1980) L167.
[18] Y.Q. Cheng, H.W. Sheng, E. Ma, Phys. Rev. B 78 (2008) 014207.
[19] H.L. Peng, M.Z. Li, W.H. Wang, C.-Z. Wang, K.M. Ho, Appl. Phys. Lett. 96 (2010) 021901.
[20] S.G. Hao, C.Z. Wang, M.J. Kramer, K.M. Ho, J. Appl. Phys. Lett. 107 (2010) 053511.
[21] M.I. Mendelev, M.J. Kramer, R.T. Ott, D.J. Sordelet, D. Yagodin, P. Popel, Philos. Mag. 89 (11) (2009) 967.
[22] X.D. Wang, S. Yin, Q.P. Cao, J.Z. Jiang, H. Franz, J.H. Jin, Appl. Phys. Lett. 92 (2008) 011902.
[23] M. Li, C.Z. Wang, S.G. Hao, M.J. Kramer, K.M. Ho, Phys. Rev. B 80 (2009) 184201.
[24] H. Tsuzuki, R. Pino, Comput. Phys. Commun. 177 (2007) 518.
[25] V. Rosato, B. Legrand, Philos. Mag. A. 59 (1989) 321.
[26] F. Cleri, V. Rosato, Phys. Rev. B 48 (1993) 22.
[27] G. Duan, D. Xu, Q. Zhang, G. Zhang, T. Cagin, W.L. Johnson, W.A. Goddard III, Phys. Rev. B 71 (2005) 224208.
[28] J. Wang, P.D. Hodgson, J. Zhang, W. Yan, C. Yang, J. Mater. Process. Technol. 209 (2009) 4601.
[29] M. Allen, D.J. Tildesley, Computer Simulation of Liquids, Oxford Science Publications, 1991.
[30] T. Fujiwara, H.S. Chen, Y. Waseda, J. Phys. F Met. Phys. 13 (1983) 97.
[31] M.I. Mendelev, D.J. Sordelet, M.J. Kramer, J. Appl. Phys. 102 (2007) 043501.
[32] E. Ma, Prog. Mater. Sci. 50 (2005) 413.
[33] J.D. Honeycutt, H.C. Andersen, J. Phys. Chem. 126 (2007) 234508.
[34] T.M. Holden, J.S. Douglas, G.C. Hallam, D. Pavuna, J. Phys. F Metal Phys. 11 (1981) 173748.